Cell

Crosslinkers and Motors Organize Dynamic Microtubules to Form Stable Bipolar Arrays in Fission Yeast

Marcel E. Janson,[1,3] Rose Loughlin,[2] Isabelle Loïodice,[1] Chuanhai Fu,[1] Damian Brunner,[2] François J. Nédélec,[2,*] and Phong T. Tran[1,*]

[1] Cell and Developmental Biology, University of Pennsylvania, Philadelphia, PA 19104, USA
[2] Cell Biology and Biophysics Program, European Molecular Biology Laboratory, 69117 Heidelberg, Germany
[3] Present address: Department of Physics and Astronomy, Vrije Universiteit, 1081 HV Amsterdam, The Netherlands.
*Correspondence: tranp@mail.med.upenn.edu (P.T.T.), nedelec@embl.de (F.J.N.)
DOI 10.1016/j.cell.2006.12.030

SUMMARY

Microtubule (MT) nucleation not only occurs from centrosomes, but also in large part from dispersed nucleation sites. The subsequent sorting of short MTs into networks like the mitotic spindle requires molecular motors that laterally slide overlapping MTs and bundling proteins that statically connect MTs. How bundling proteins interfere with MT sliding is unclear. In bipolar MT bundles in fission yeast, we found that the bundler ase1p localized all along the length of antiparallel MTs, whereas the motor klp2p (kinesin-14) accumulated only at MT plus ends. Consequently, sliding forces could only overcome resistant bundling forces for short, newly nucleated MTs, which were transported to their correct position within bundles. Ase1p thus regulated sliding forces based on polarity and overlap length, and computer simulations showed these mechanisms to be sufficient to generate stable bipolar bundles. By combining motor and bundling proteins, cells can thus dynamically organize stable regions of overlap between cytoskeletal filaments.

INTRODUCTION

The bundling of MTs is a crucial step in the formation of MT arrays in interphase and mitotic cells. Lateral contacts between MTs are seen in diverse structures like the spindle midzone, axons, developing muscle cells, cilia, and epithelial cells. The polarity of MT contacts is directly related to the function of MT networks in regulating cell polarity: bundles of parallel MTs in axons provide a directional cue for vesicle transport (Heidemann et al., 1981), and antiparallel MT contacts in the spindle-midzone are essential to the bipolarity of the mitotic spindle (Sharp et al., 2000).

In general, processes that regulate the polarity of MTs are not well understood. Centrosomes play a role by grouping MT minus ends together such that neighboring MTs in their asters are parallel. Yet in many systems MTs are nucleated from randomly dispersed nucleation sites and can still form polarized arrays (Janson et al., 2005; Mahoney et al., 2006; Murata et al., 2005). Components of mitotic extracts, for example, organize MTs into bipolar arrays in the complete absence of centrosomes (Heald et al., 1996). MT bundling proteins presumably contribute to polarity establishment by selectively bundling parallel or antiparallel MTs. However, the existence of such selectivity was hitherto not demonstrated for static crosslinking proteins like NuMA or the spindle-midzone-protein PRC1. Instead, work has focused on molecular motors that exert directed forces to dynamically sort MTs into polarized MT arrays. Motors have multiple MT binding sites or form oligomeric complexes to crosslink and transport MTs along MTs (Sharp et al., 2000). The kinesin motor MKLP1 (kinesin-6) was shown to interact selectively with antiparallel MTs in the spindle midzone during mitosis (Nislow et al., 1992), while CHO2 (kinesin-14) can induce the formation of parallel MT bundles (Sharp et al., 1997). In the midzone of spindles, plus-end-directed motors like Eg5 (kinesin-5) and MKLP1 are believed to slide plus ends of antiparallel overlapping MTs toward each other, while minus-end-directed motors (kinesin-14) were proposed to generate balancing opposite forces to establish stable MT contacts. Computer simulations, however, showed that such a scheme may work only if motor domains are able to halt at MT ends, which is in effect a mixed activity of static MT bundling and active sliding (Nedelec, 2002). A combination of static MT-end crosslinkers and molecular motors was furthermore proposed to be required for stably focusing MT minus ends into asters in the absence of centrosomes (Chakravarty et al., 2004). Combining static crosslinking activity with motors thus seems to increase the ability of dynamic systems to generate stable MT contacts with the correct polarity. How bundling and sliding activity are tuned to one another such that networks neither become too rigid nor too dynamic is unknown. Adding

motor proteins to statically bundled MT networks can cause separation of MTs (Maresca et al., 2005), so regulatory mechanisms are needed to establish lasting MT connections. Clearly, a good understanding of these processes requires detailed knowledge of the MT binding properties of bundlers and motors with emphasis on MT-end binding and crosslinking polarity preference.

Both motor and bundling proteins are required for the construction of three to four bipolar MT bundles along the long axis of rod-shaped fission yeast cells—*Schizosaccharomyces pombe*—in interphase (Brunner and Nurse, 2000; Drummond and Cross, 2000; Tran et al., 2001; Figure 1A; see Movie S1 in the Supplemental Data available with this article online). Like the spindle midzone, these bundles contain antiparallel contacts between MTs. MTs within each bundle are oriented such that their plus ends typically grow at 2 to 3 μm/min toward the nearest cell tip, whereas their nongrowing minus ends are bundled by ase1p (the yeast homolog of PRC1) to form a bundle-midzone of crosslinked antiparallel MTs in the central cell region (Loiodice et al., 2005; Yamashita et al., 2005). During mitosis, ase1p bundles antiparallel MT plus ends in the spindle midzone. So, although the orientation of MTs is reversed compared to interphase bundles, the same protein is involved in the regulation of bipolarity (Loiodice et al., 2005). It was shown that interphase bundles are dynamic structures from which individual MTs are removed by disassembly, while new MTs are added by nucleation from γ-tubulin complexes along the length of preexisting MTs (Carazo-Salas et al., 2005; Janson et al., 2005). A minus-end-directed kinesin-14, klp2p, transports new MTs toward the bundle midzone, but how their minus ends subsequently become stably embedded in the bundle midzone is not understood. Deletion of *ase1* inhibits the bundling of MTs into a bundle midzone (Loiodice et al., 2005; Yamashita et al., 2005) whereas deletion of *klp2* inhibits MT sliding (Carazo-Salas et al., 2005). Ase1p and klp2p are therefore the dominant, and possibly the only, bundler and motor involved in MT organization, making *S. pombe* a suitable model system to study the effect of bundling proteins on MT sliding.

Here, we demonstrate that the MT bundling properties of ase1p and klp2p suffice to sort dispersedly nucleated MTs into bipolar MT arrays. We show that ase1p contributes to bipolarity by selectively crosslinking antiparallel MTs. Newly nucleated MTs are therefore oriented antiparallel to preexisting MTs and are transported toward the bundle midzone by klp2p-mediated sliding. Sliding and bundling forces are regulated such that only short, newly nucleated, MTs are transported. As part of this regulation, ase1p accumulated all along the length of bundled MTs, whereas klp2p gathered at MT plus ends in a length-independent manner. We argue that similar length-dependent and -independent forces more generally regulate MT overlap. Thus, our analysis identifies MT end binding and polarity specificity as key elements to the organization of MT arrays.

RESULTS

Klp2p Only Pulls at MT Plus Ends

The movement and dynamics of individual MTs within bundles can be visualized using kymographs (Sagolla et al., 2003). The kymographs shown in this article display the intensity of fluorescently tagged tubulin along straight or slightly bend MT bundles as a one-dimensional horizontal array of pixels with corresponding intensity variations. Repeating this procedure for each frame of a time-lapsed movie generates a two-dimensional image with time along the vertical dimension. Figure 1B shows a kymograph of a wild-type cell expressing small amounts of GFP-tubulin (*atb2*) in addition to endogenous tubulin expression. Typical MTs that grew from and subsequently shortened back to the cell center form triangles of increased intensity (Figure 1B, an example is colored red). Shortening continued until the MTs were completely disassembled. Appearing speckles (Figure 1B, yellow circle), points of increased and decreased intensity along MTs caused by the nonuniform incorporation of GFP-tubulin, form vertical lines in kymographs (Waterman-Storer et al., 1998) that often allowed for the identification of the three sides of the triangle: nondynamic minus end (Figure 1B, label 6), growing plus end (Figure 1B, label 1), and shortening plus end (Figure 1B, label 2). A kymograph of a complete bundle can be viewed as a superposition of several MT triangles that gives rise to areas with increased intensity. Most MT overlap was seen in the bundle midzone between antiparallel MT minus ends (Figure 1B, label 3), but additional overlap zones were occasionally created by two parallel MTs emanating from the bundle midzone (Figure 1B, label 5). Furthermore, new MTs were nucleated (Figure 1B, label 4) and transported along existing MTs toward the bundle midzone. One example is highlighted in green (Figure 1B), for which sliding can be observed relative to a static speckle on the underlying MT (Figure 1B, yellow dots). Nucleated MTs are oriented antiparallel with respect to the underlying MTs, such that once their plus ends cross the bundle midzone, they eventually grow with the correct polarity toward the closest cell end (Janson et al., 2005). In contrast to the sliding of new MTs, overlapping MT minus ends within the bundle midzone did not slide relative to each other (Figure 1B, label 3), raising the question of how sliding is regulated.

To directly observe the formation of a stable bundle midzone by just two MTs, we looked for rare events in which one MT was nucleated along a single MT. In Figure 1C, nucleation takes place 4.0 μm away from an existing minus end. The sliding of the novel minus end gradually slowed as the new MT elongated and completely stalled after sliding a total length of 1.2 μm. Meanwhile, its plus end continued growing and eventually extended beyond the minus end of the underlying MT (Figure 1C, yellow circle). The resultant bundle midzone was 2.8 μm long. Figure 1D (white circle) shows a second example for which nucleation occurs only 1.2 μm away from the existing minus end, and movement stops after 0.4 μm of
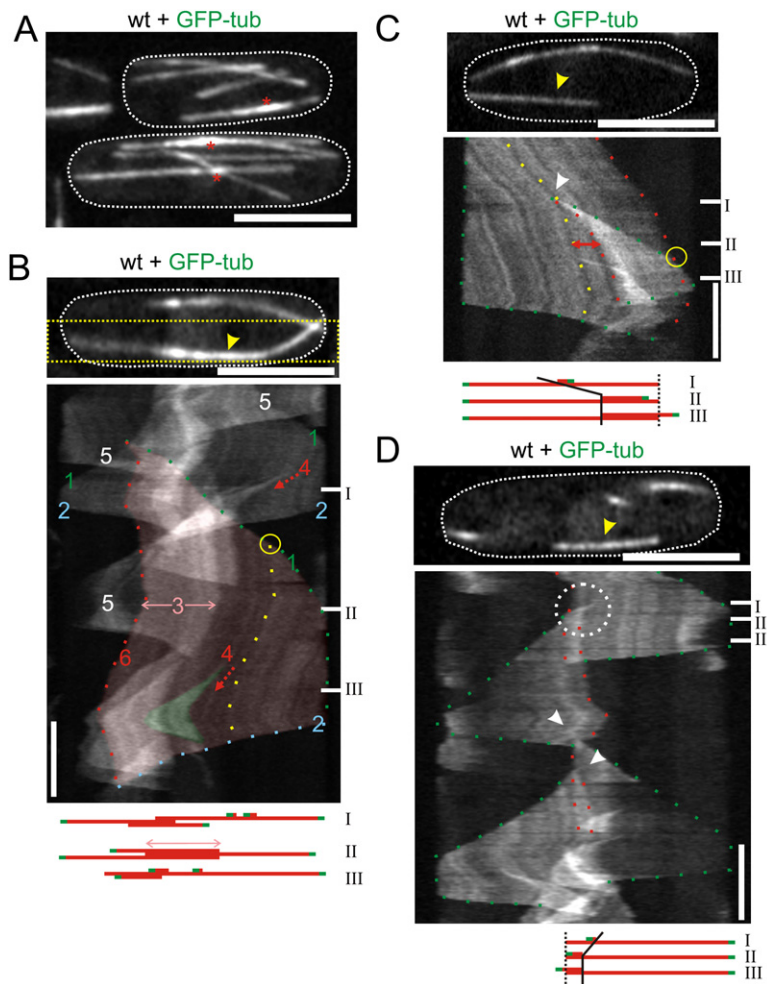
Figure 1. Selective Relative Sliding of MTs in Fission Yeast

Scale bars, 5 μm and 2 min.

(A) Whole-cell projected image (10 confocal planes spaced by 0.5 μm) of MT bundles with visible bright bundle midzones indicated by an *.

(B) Top: single-plane confocal image of two MT bundles. Bottom: kymograph generated from the yellow-boxed area. The intensity variations along the MT bundle in the top image (yellow arrow) can be recognized in the first line of the kymograph. Growth and shortening of MTs gives rise to triangular patterns in the kymograph—two examples are colored red and green. See text for explanation of the labels. MT sliding (red arrows) occurred after the nucleation of new MTs (label 4). A schematic interpretation of the MTs in the bundle is depicted for selected time points (white bars) with MT plus ends indicated in green. MTs are nucleated antiparallel on top of existing MTs.

(C) Kymograph of a MT nucleated on a rare single MT. Green, red, and yellow dotted lines indicate plus and minus ends and speckles, respectively. After nucleation sliding occurred over 1.2 μm (red arrow). The cartoon shows that sliding effectively stopped before the new plus end passed the old minus end (yellow circle).

(D) Same as (C), but MT nucleation occurred close to an existing minus end. The encircled MT is described in the text; two similar events are observed at later time points (white arrowheads). The cartoon shows that MT sliding stopped when the new plus end passed the old minus end.

sliding. The resultant bundle midzone of only 0.8 μm shows that midzone length varies significantly with the location of MT nucleation.

To understand the forces involved in the generation of a bundle midzone, we investigated the distribution of motor proteins along MTs by constructing two-color kymographs of simultaneously imaged klp2-GFP and mRFP-tubulin (Figures 2A and S1A; Movies S3 and S5). Interestingly, klp2-GFP tracked plus ends of growing MTs and was notably absent from MT minus ends. Sliding forces between overlapping MTs are therefore generated solely at MT plus ends, explaining the abrupt stop and constant overlap of the nucleated MT in Figure 1D once its plus end passed the underlying MT. Within mature bundles with more than two MTs, we furthermore noticed that no MT minus ends were pushed out of the bundle midzone by parallel MT sliding, suggesting that—in contrast to antiparallel sliding of new MTs—klp2p is unable to bundle and slide parallel MTs (see schematic in Figure 2A). In support of this we noticed that (1) parallel MTs can splay apart within bundles (Figure 2B and Movie S4) and (2) the plus ends of parallel-growing MTs in kymographs did not

slide relative to each other (Figures 2A and S1A). The MT binding properties of klp2p are thus tailored to arrange MT minus ends stably into a small bundle midzone.

Ase1p Polarizes MT Networks by Selective Bundling of Antiparallel MTs

The splaying of parallel MTs near cell ends (Figure 2B) suggests that MT bundling is restricted to the bundle midzone. To investigate localized bundling by ase1p, we constructed kymographs of ase1-GFP and mRFP-tubulin. Ase1-GFP indeed localized to the bundle midzone but also all along the length of MTs that were nucleated along preexisting MTs (Figure 2C and Movie S6). Both of these regions contain antiparallel MT contacts, suggesting that (1) ase1p localizes primarily to antiparallel MTs and (2) MTs within the bundle midzone are held together by antiparallel contacts. To test whether this polarity preference is an intrinsic property of ase1p, we added bacterially expressed GST-ase1p to dynamic MTs grown from purified tubulin. Encounters between growing MT ends and existing MTs resulted in either crossing or bundling, depending on the interaction angle and polarity (Figures 3A
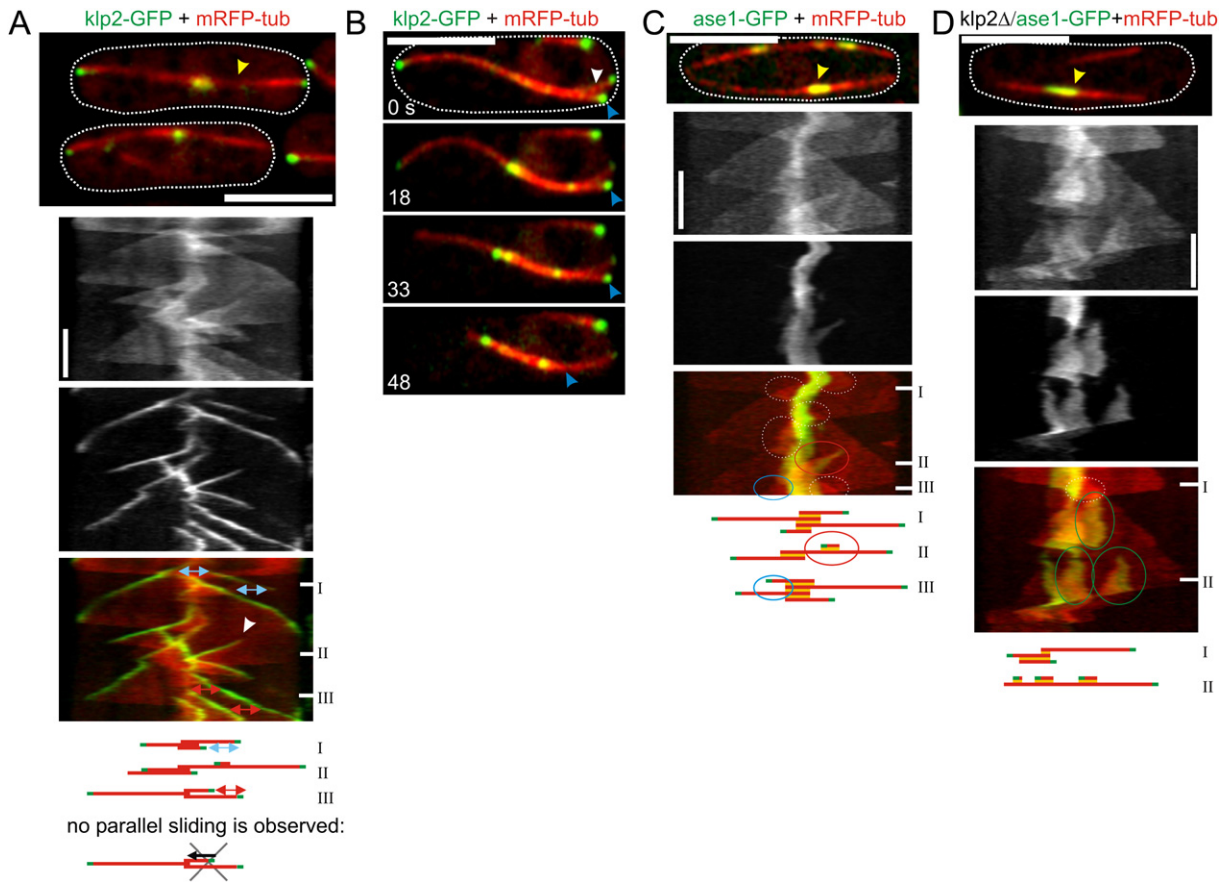
Figure 2. Klp2p Targets MT Plus Ends and ase1p Targets Antiparallel MTs

Scale bars, 5 μm and 2 min.

(A) Kymographs of a cell expressing klp2-GFP (middle kymograph) and mRFP-tubulin (upper kymograph) showing plus-end tracking of klp2-GFP to existing and novel (white arrowhead) MTs. The distance between plus ends of parallel MTs remains constant (blue and red arrows).

(B) Image series of a bundle that initially, given klp2p-GFP localization, contains one MT growing to the left and two parallel MTs growing to the right (t = 0 s). The bundle buckles strongly (t = 18 s) due to forces generated by MT growth at cell ends, and consequently, the two parallel MTs splay apart (white arrowhead) while the bundle midzone stays intact. The left MT has a catastrophe (t = 33 s) followed by one of the parallel MTs (blue arrowhead; t = 48 s). Klp2p-GFP does not localize to shortening plus ends.

(C) Kymograph of a cell expressing ase1-GFP and mRFP-tubulin revealing strong ase1p targeting to the bundle midzone and to a newly nucleated MT (red circle). Ase1p localization to this MT is lower when the same MT grows along a parallel MT on the other side of the bundle-midzone (solid blue circle). Dashed white circles indicate additional regions of parallel overlap. Ase1p localization is indicated in ochre in the schematic interpretation.

(D) Kymograph of a *klp2Δ* cell expressing ase1-GFP and mRFP-tubulin revealing klp2p-independent targeting of ase1p to nucleated MTs (green circles). These MTs are still oriented antiparallel to underlying MTs (Figure S1B) but do not slide in the absence of klp2p. All displayed images were acquired with single-plane confocal microscopy.

and 3B; Movies S8 and S9). For angles smaller than 15 degrees, the bundling of antiparallel MTs was 9.4 times more likely than the bundling of parallel MTs, and bundling probabilities decreased for higher interaction angles. MTs in this assay bound to the coverslip due to surface binding of GST-ase1p. Consequently, MTs had to bend locally under considerable angles in order to bundle with existing MTs (Movie S8). The required bundling forces can thus be exerted by GST-ase1p along antiparallel MTs but less so along parallel MTs.

The bundling of MTs by ase1p homologs requires the formation of protein oligomers to bring together two or more MT binding domains; homologs in budding yeast

(Schuyler et al., 2003) and plants (Smertenko et al., 2004) were proposed to form dimers, and the mammalian homolog PRC1 is believed to form even higher-order oligomers (Mollinari et al., 2002; Zhu et al., 2006). Dimer formation by the N terminus of ase1p (Figure 3C) and immunoprecipitation of HA-tagged ase1p and GFP-tagged ase1p (Figure 3D) showed that fission yeast ase1p oligomerizes. Preferential antiparallel bundling may therefore be enforced by a rigid antiparallel positioning of MT binding domains within ase1p oligomers. Interestingly, the N terminus of ase1p has a predicted spectrin domain (InterPro database) that was required for oligomerization (Figures S3 and 3D). Spectrin repeats form antiparallel
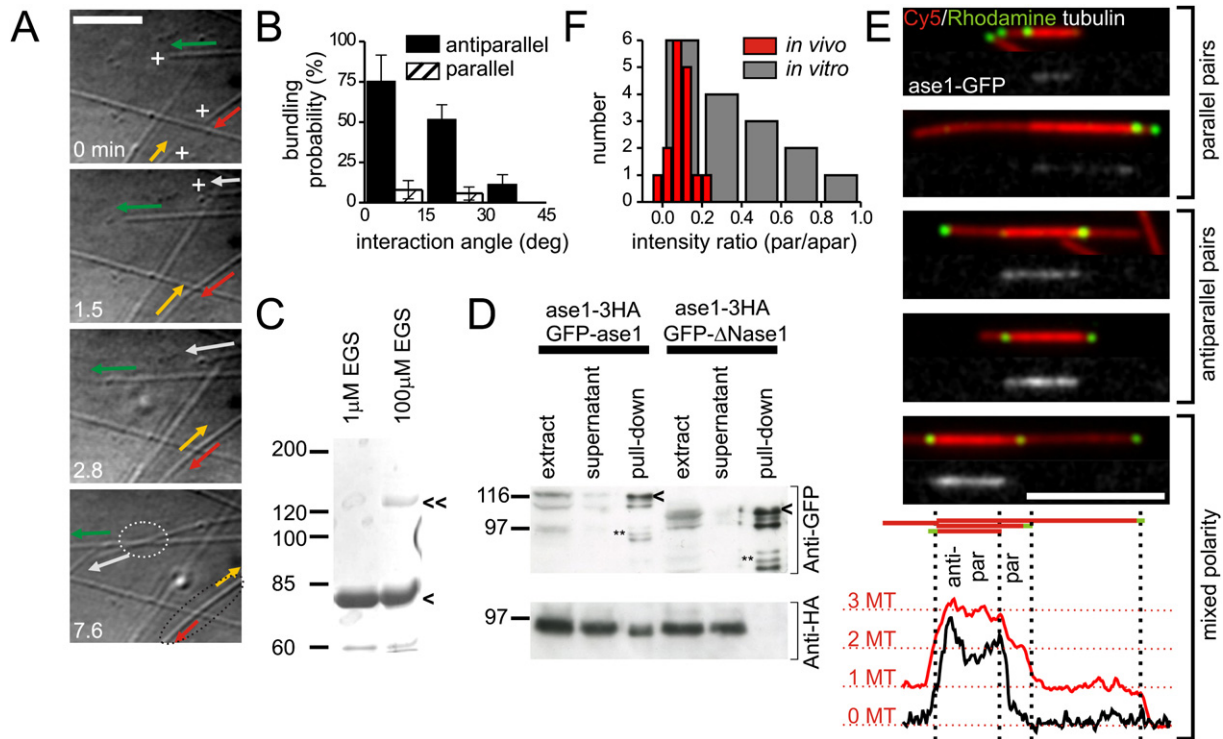
Figure 3. Specific Interactions of ase1p with Antiparallel MTs In Vitro

Scale bars, 5 μm.

(A) Differential interference contrast (DIC) image series of growing MT plus ends (indicated by arrows and + symbols) emanating from axonemes (axonemes are out of view). In the presence of GST-ase1p, growing MT plus ends either cross without bundling (white circle; green and white MTs; t = 7.6 min) or bundle together (black circle; the plus ends of the red and yellow MTs meet at t = 1.5 min and then grow along each others path). Bundles have a slightly higher contrast than single MTs, which allows for the observation of growing MTs within bundles (Movie S8). Note that the green and white MTs are parallel and the red and yellow MTs are antiparallel.

(B) Bundling probability for parallel (n_{total} = 83; 25,35, and 23 in subsequent bins) and antiparallel MTs (n_{total} = 80; 12,41, and 27 in bins) as a function of interaction angle (±SD). No parallel bundling was seen above 30 degree angles.

(C) Coomassie-stained SDS-PAGE gel of the purified N terminus of ase1p (first 483 amino acids; M_w = 56 kDa) crosslinked with EGS. At 100 μM EGS, a band (≪) is visible at twice the weight of the monomer (<).

(D) Western blot showing ase1-3HA immunoprecipitation with GFP-ase1p but not with GFP-ΔNase1p from cell extracts. Principle bands are marked with <.

(E) Three-color wide-field fluorescence images showing preferential localization of His-ase1-GFP (lower panels) to regions of overlapping MTs (upper panels). All images are from the same sample and have the same contrast setting. MT plus ends are visualized as green dots (Rhodamine channel). The lower image has three MTs of mixed polarity, giving rise to regions of parallel and antiparallel overlap as indicated. Linescans of background-subtracted fluorescence levels were used to quantify MT number (Cy5-channel) and relative His-ase1-GFP levels.

(F) Histograms of the ratio of ase1-GFP fluorescence along parallel MTs and antiparallel MTs in vivo (n = 16) and in vitro (n = 16).

dimers in muscle α-actinin, which bundles antiparallel actin filaments in muscle Z disks (Djinovic-Carugo et al., 1999). The structural basis of MT and actin bundling may therefore be in part conserved.

Ase1p Autonomously Localizes to Interdigitated MTs

How do motor and bundling proteins like klp2p and ase1p target specific locations within MT networks? Similarly to kinesin-14 motors in other systems (Goshima et al., 2005; Sproul et al., 2005), klp2p may be recruited to MT plus ends by specialized plus-end-tracking proteins like EB1 or Cik1. Bundling proteins may depend on motor proteins for their localization; NuMA and PRC1 were proposed

to associate with oppositely directed motors (dynein [Merdes et al., 1996] and Kif4 [Zhu and Jiang, 2005]) for transport along MTs toward the spindle poles and the spindle midzone, respectively. Could a minus-end-directed motor transport ase1p along MTs toward antiparallel MTs in the bundle-midzone? The only minus-end-directed motor shown to affect bundle organization is, however, klp2p (Carazo-Salas et al., 2005), and ase1-GFP remains associated with antiparallel MTs in klp2Δ cells (Figure 2D and Movie S7). To investigate whether ase1p localizes autonomously to antiparallel MTs, we bundled polarity-marked stabilized MTs with bacterially expressed His-ase1-GFP. MTs were bound to the coverslip of a flowcell, and bundles with various amounts of MTs could be observed

(Figure 3E). The majority of MTs in bundles of two MTs were antiparallel (66% ± 6%, ±SD, n_{total} = 61), but the orientational preference was smaller than observed previously (Figure 3B). In the current assay, weak nonspecific interactions between ase1p and MTs may have bundled parallel MTs in solution because no large forces were required to bend MTs. The average fluorescence intensity of His-ase1-GFP along parallel MTs was 35% ± 8% (±SEM; n = 16) of that along antiparallel MTs (n = 28) (Figure 3F). Furthermore, targeting to single MT regions (n = 44) in bundles was very dim and often undetectable (3.4% ± 1.5%, ±SEM, of average intensity along antiparallel MTs), indicating a large affinity of ase1p for overlapped MTs and in particular for antiparallel overlapping MTs. A similar enrichment at bundled regions was observed with GST-tagged ase1-GFP, indicating that this property is independent of the protein tags used (data not shown). To compare these results with ase1p localization in vivo, we quantified the intensity of ase1-GFP along two parallel or two antiparallel MTs using kymographs of cells that coexpress mRFP-tubulin (Figure 2C). In vivo, the intensity of ase1-GFP along two parallel MTs, as judged from two-color kymographs, was on average 9% ± 1% (±SEM; n = 16) of that along two antiparallel MTs in the same bundle (Figure 3F), and ase1p-GFP targeting to single MTs could not be detected. The larger in vivo orientational preference may yield a strong bias toward the formation of antiparallel MT arrays in living cells. This would explain observations in MT nucleation deficient *mto2Δ* cells, in which only interactions between antiparallel treadmilling MTs generate bundling (Janson et al., 2005). Part of the observed differences between in vivo and in vitro measurements may be related to differences in ase1p-GFP concentration. In support of this, we note that specific targeting was inhibited in vitro by further increasing the ase1p-GFP concentration, which yielded significant localization of ase1p-GFP to single MTs (up to 40% of targeting to overlapped regions; data not shown). Similarly, overexpression of ase1p-GFP in fission yeast yielded localization to single MTs in vivo (data not shown). Furthermore, we note that specific interactions of ase1p with antiparallel MTs, and possible nonspecific interactions with parallel MTs will depend to varying degrees on ionic strength. Nonspecific interactions are likely screened in the cell, increasing the importance of specific interactions.

We reasoned that the multiple MT binding domains within ase1p-oligomers may be oriented such that, due to steric effects, simultaneous binding of all domains to the same MT is prevented, whereas binding to two antiparallel MTs is allowed (Figure 4A). Interactions with overlapped MTs may therefore generate strong multiple bonds that compete ase1p away from single MTs. To find support for this localization mechanism, we expressed a monomeric ase1p mutant in *ase1Δ* cells. GFP-ΔNase1p (ase1p without the putative spectrin domain) could not recover the unbundled-MT phenotype of *ase1Δ* cells (Loiodice et al., 2005) and localized dimly along the full length of MTs (Figure 4B and Movie S10). Localization and MT bun-
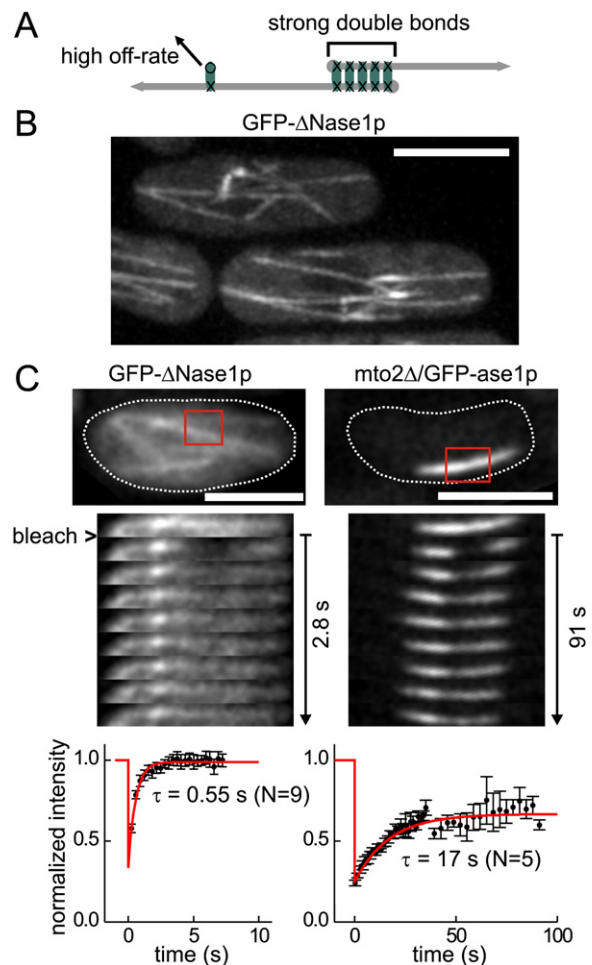

Figure 4. Mechanism of Autonomous ase1p Localization to Overlapping MTs

Scale bars, 5 μm.
(A) Proposed localization mechanism of ase1p (drawn as a dimer with two MT binding sites). The second binding site (O symbol) is sterically hindered from binding, except along two antiparallel MTs.
(B) Whole-cell projected confocal image of GFP-ΔNase1p along MTs in *ase1Δ* cells. MTs are unbundled compared to wild-type cells (Figure 1A).
(C) FRAP in *ase1Δ* cells expressing GFP-ΔNase1p (left) and in *mto2Δ/ase1Δ* cells expressing GFP-ase1p (right). One cropped, prebleach confocal image is shown with the FRAP area indicated. The average recovery of the fluorescence signal (±SEM) was fitted with a single exponential.

dling are thus directly dependent on ase1p oligomerization, which itself may be regulated by phosphorylation like recently demonstrated for PRC1 (Zhu et al., 2006). To investigate whether the dynamics of binding between ase1p oligomers and MTs is consistent with the proposed localization mechanism, we performed fluorescence recovery after photobleaching experiments (FRAP) on GFP-ΔNase1p along single MTs (one MT binding domain per ase1p monomer) and GFP-ase1p along bundled MTs (multiple MT binding domains per ase1p oligomer).

GFP-ΔNase1p expressed in *ase1Δ* cells recovered quickly with a time constant of 0.55 ± 0.05 s (n = 9; ±SEM; Figure 4C and Movie S11). For GFP-ase1p expressed in *ase1Δ/mto2Δ* cells, we measured a significantly longer time constant of 17.0 ± 1.5 s (n = 5; Figure 4C and Movie S12). The relatively long bundled regions in *mto2Δ* cells allowed for partial bleaching of ase1p stretches (Janson et al., 2005), which helped to distinguish between GFP-ase1p recovery and the generation of new bundled regions. An intensity-based analysis of the fractional coverage of MTs by GFP-ΔNase1p and GFP-ase1p allowed for an estimation of molecular rate constants from the measured time constants (Figure S2). Approximately one out of six available binding sites along MTs were occupied by GFP-ΔNase1p, implying that the molecular off-rate of GFP-ΔNase1p was significantly higher than $1/0.55\ s = 1.8\ s^{-1}$, whereas the off-rate of GFP-ase1p at regions of overlap was close to $1/17.0\ s = 0.059\ s^{-1}$. Brief interactions involving a single MT binding domain may therefore allow ase1p to quickly "scan" MTs for overlapped regions and subsequently bind tightly.

Ase1p-Attenuated klp2p-Sliding Suffices to Generate Bipolarity

Are sliding forces generated at MT plus ends by klp2p and ase1p-dependent bundling forces sufficient to organize MT bundles? Two observations, important for our understanding of the forces involved in MT organization, indicated that sliding forces are negatively affected by ase1p bundling. First, the average sliding velocity of nucleated MTs was higher in *ase1Δ* cells than in wild-type cells (11.3 ± 0.5 μm/min, ±SEM, versus 5.5 ± 0.25 μm/min [Janson et al., 2005]; Figure S1C). Second, the velocity of new MTs slowed gradually during their elongation (red dots in Figures 1B and 1C), which can be explained by a constant number of motors at the plus end (Figure 2A) that are slowed down by a length-dependent increase of bundling proteins (see model, Figure 6A). We quantified this latter effect by analyzing 20 kymographs of wild-type cells in which MTs moved along a secondary MT without interactions with tertiary MTs (including Figure 1C). From these, we measured the velocity of minus ends versus MT length (Figure 5C). Relative to the underlying MT, the shortest MTs (average length 0.26 μm) moved at 4.6 ± 0.5 μm/min (±SEM), whereas the longest analyzed MTs (average length 2.1 μm) were nearly stalled (0.6 ± 0.1 μm/min). The slow speed of longer MTs explains why, as in Figure 1C, MTs can stop before the motors at their plus end pass the minus end of the underlying MT. In *klp2Δ* cells, even short MTs did not slide (Figure 5C; n = 13), providing further evidence that klp2p is the primary molecular motor involved in MT sliding in interphase.

We used Cytosim, a computer simulation, to study the requirements for bundle assembly with competing sliding and friction forces. Cytosim solves the Langevin equation at low Reynolds number for MTs and treats events such as protein binding, nucleation, and catastrophe as stochastic (Nedelec, 2002). We simulated bundling of dynamic MTs using three different combinations of ase1p- and klp2p-

like complexes in a confined geometry that mimicked the shape of a fission yeast cell (Figure 5A). Previously reported attachments of MTs to the nuclear envelope were not modeled, in agreement with recent data showing that these interactions are transient and not required for the self-organization of MT bundles (Carazo-Salas and Nurse, 2006; Daga et al., 2006). Model 1 was in accordance with the experimentally observed characteristics of ase1p and klp2p: ase1p had two identical binding domains with the restriction that it could crosslink only antiparallel MTs. Klp2p was a minus-end-directed motor whose cargo was limited to the plus end of a growing MT and whose velocity was linearly dependent on the applied load. The velocity at zero load (10.8 μm/min; Table S3) was chosen to model the low-load condition in *ase1Δ* cells. The simulation was seeded with an initial MT and included nucleation complexes that were active only while bound laterally to a preexisting MT. Nucleations and catastrophes resulted in an average of five bundled MTs (Figures 5B and 5E and Movie S15) that matched the following experimental observations: (1) nucleated MTs were transported along existing MTs toward the center of the bundle with a length-dependent velocity that matches the experimental length-velocity curve well (Figure 5C); (2) a bundle midzone of antiparallel MTs formed and fluctuated in size but kept a centered position; (3) compressive forces generated by MT polymerization against cell ends buckled MTs, but the bundle midzone resisted compression; (4) bundles separated and fused on occasion; and (5) relative to the cell center, 84% of the MTs were oriented outwards, comparable to 90% measured in vivo (Carazo-Salas et al., 2005). Model 1 thus successfully reproduced functional bundles, demonstrating that the opposing forces of motors and bundlers are sufficient to generate stable bipolar MT bundles from MTs nucleated randomly along existing MTs. To test whether model 1 represents the minimal necessary assumptions, model 2 further simplified the assumptions by allowing ase1p to bind regardless of MT orientation. This resulted in MT bundles with less antiparallel overlap, less symmetry in the bundle-midzone, and with a reduced ability to focus minus ends in the center (Figures 5A, 5D, and S5 and Movie S16), demonstrating that the specificity of ase1p optimizes bundle organization. Quantitative differences between the models (Figures 5A and 5D) should be related to the unbundled model, containing no bundlers or motors and consisting of nucleation in random locations, which serves as the paradigm of MT disorganization and isolates the effect of motors and bundlers on MT organization (Movie S18). In model 3, we removed klp2p, which often resulted in an overlap region that was wide and reduced to two MTs (Figures 5A, 5D, and S6 and Movie S17). Klp2p is thus required for strengthening and stabilizing the bundle by bringing more MTs into the antiparallel MT overlap region, in agreement with observations of decreased bundle stability and wider overlap regions in *klp2Δ* cells (Carazo-Salas et al., 2005). In model 3, the number of outward-directed MTs was lowered to 78%
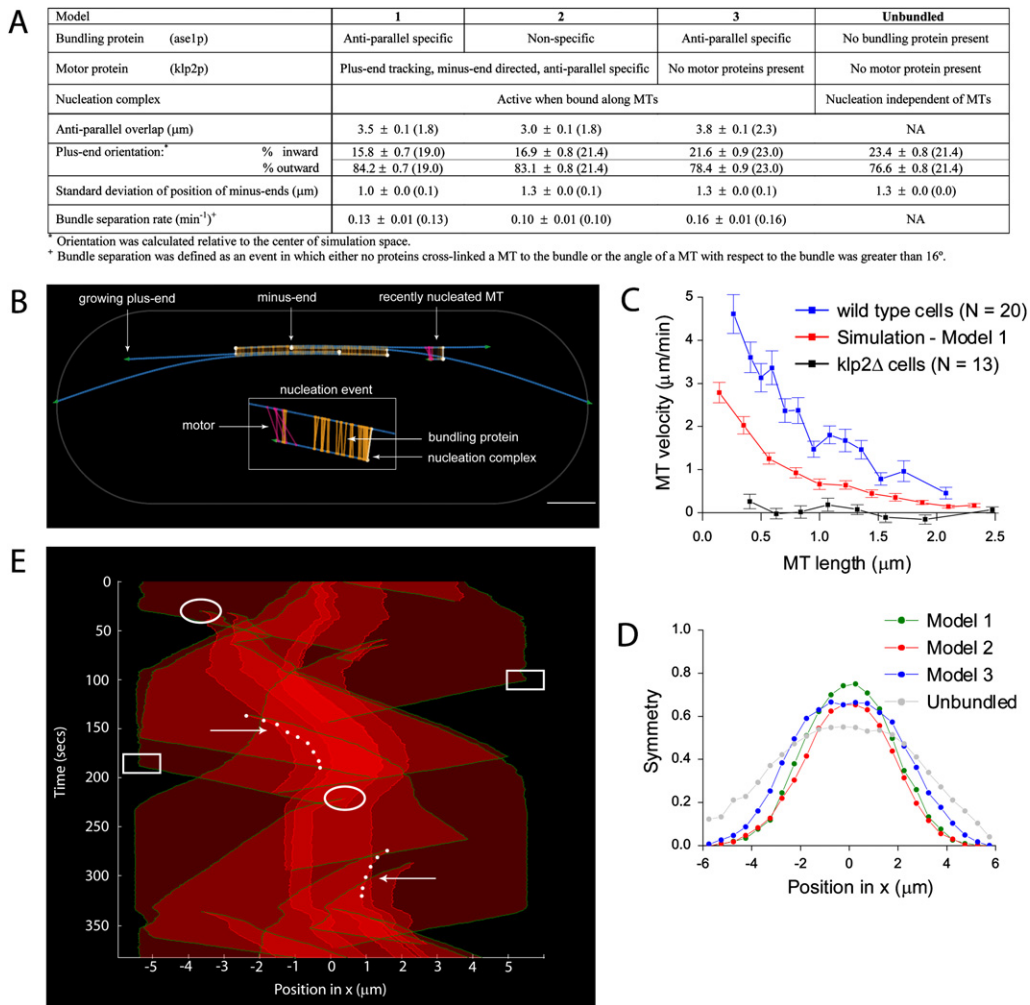
Model	1	2	3	Unbundled
Bundling protein (ase1p)	Anti-parallel specific	Non-specific	Anti-parallel specific	No bundling protein present
Motor protein (klp2p)	Plus-end tracking, minus-end directed, anti-parallel specific		No motor proteins present	No motor protein present
Nucleation complex	Active when bound along MTs			Nucleation independent of MTs
Anti-parallel overlap (μm)	3.5 ± 0.1 (1.8)	3.0 ± 0.1 (1.8)	3.8 ± 0.1 (2.3)	NA
Plus-end orientation:* % inward	15.8 ± 0.7 (19.0)	16.9 ± 0.8 (21.4)	21.6 ± 0.9 (23.0)	23.4 ± 0.8 (21.4)
% outward	84.2 ± 0.7 (19.0)	83.1 ± 0.8 (21.4)	78.4 ± 0.9 (23.0)	76.6 ± 0.8 (21.4)
Standard deviation of position of minus-ends (μm)	1.0 ± 0.0 (0.1)	1.3 ± 0.0 (0.1)	1.3 ± 0.0 (0.1)	1.3 ± 0.0 (0.0)
Bundle separation rate (min⁻¹)†	0.13 ± 0.01 (0.13)	0.10 ± 0.01 (0.10)	0.16 ± 0.01 (0.16)	NA

* Orientation was calculated relative to the center of simulation space.
† Bundle separation was defined as an event in which either no proteins cross-linked a MT to the bundle or the angle of a MT with respect to the bundle was greater than 16°.

Figure 5. Computer Simulation of Bundle Formation by ase1p and klp2p

(A) The components and experimental results ±SEM (SD) for models 1, 2, 3, and unbundled.
(B) Simulation result displaying the bundling proteins, motor proteins, nucleation complexes and area of confinement. MTs are displayed with small added vertical displacements to aid viewing, but are simulated as infinitely thin lines. Scale bar, 1 μm.
(C) Average sliding velocity of MTs as a function of their length. Velocity was analyzed every 5 s and binned according to MT length (±SEM).
(D) Average local bundle symmetry, defined by $S = 4\,RL/(R+L)^2$, where R and L are the number of MTs pointing right and left, respectively. Ideal bundles have $S = 1$ in a small bundle midzone and $S = 0$ near cell ends. Relative to the unbundled model, bundling activity increases symmetry in the central region: model 1 attains the highest symmetry, model 2 has the lowest symmetry, and model 3 the widest symmetric region. Position is relative to the average position of the minus ends.
(E) Simulated kymograph of model 1. White circles indicate nucleation events (MT plus ends in green and MT minus ends in light red). MT growth, sliding (white arrow), and catastrophe events (white box) are observed. The velocity of sliding decreases with MT elongation (white dots). Sliding between parallel MTs does not occur.

(Figure 5A), comparable to the value of 75% measured in klp2Δ cells, showing that model and cell are about equally sensitive to the removal of klp2p.

DISCUSSION

In this study, we demonstrate that a bipolar MT array can be organized in the absence of centrosomes through the action of a MT bundler (ase1p) and a MT motor (klp2p). The MT binding properties of these proteins have evolved such that a subpopulation of short MTs can slide along preexisting MTs to attain their correct localization within MT bundles.

Bias in Crosslinking Polarity Aids Protein Localization and MT Self-Organization
We found that the MT bundling protein ase1p has the inherent ability to distinguish between parallel and anti-parallel MTs. A similar specificity had been proposed for the binding of α-actinin isoforms to actin filaments (Meyer and Aebi, 1990), but the potential of polarity specificity of cytoskeletal bundling proteins to control self-organization
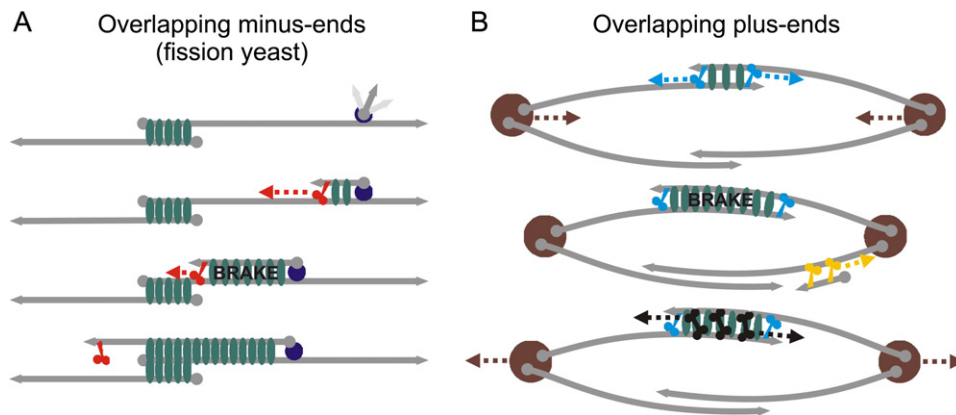
Figure 6. Model for MT Organization with Competing Sliding and Friction Forces

(A) MT plus ends are indicated by arrow heads, minus ends by spheres. MT nucleation along interphase bundles occurs from MT-bound nucleation complexes (purple). After nucleation, MTs are stabilized in the antiparallel configuration by polarity-specific ase1p (green). The minus-end-directed kinesin-14 klp2p (red) subsequently transports MTs to the bundle midzone. As the new MT grows, additional ase1p binds, increasing the friction against a length-independent number of motors at MT plus ends. Consequently, the speed of transport decreases and finally becomes zero when motors lose contact with antiparallel MTs.

(B) Possible mechanisms, based on length-dependent and -independent forces, for the regulation of overlap between antiparallel overlapping MT plus ends. The bundling of antiparallel MTs by ase1p (observed in anaphase spindles) would not interfere with the focusing of parallel MTs toward the spindle poles by minus-end-directed motors (yellow). Other minus-end-directed motors may specifically bind to MT plus ends (blue) and pull poles together with an overlap-independent force. An increase in overlap recruits additional ase1p proteins, generating friction that resists MT sliding and slows down pole-to-pole motion. Plus-end-directed motors (black) may bind in a length-dependent manner along MTs, a process potentially regulated by the binding of motors to ase1p. For large overlap, enough plus-end-directed motors may bind to push the poles outward. An equilibrium overlap can then exist at which forces generated by plus- and minus-end-directed motors and ase1p are balanced.

processes in cells has remained largely unaddressed. Because of its polarity preference and its weak binding to single MTs, ase1p localizes with high fidelity to antiparallel interdigitated MTs. Interestingly, ase1p localizes to overlapping minus ends during interphase and overlapping plus ends in anaphase spindles. The difference in localization in both cell stages may be purely determined by molecular motors and geometry effects that bring either antiparallel minus ends (interphase/klp2p) or plus ends together (anaphase/opposing spindle poles; Figure 6). The specialized MT binding properties of ase1p/PRC1 may aid the localization of various proteins. Molecular binding partners of PRC1 in mitosis, which intriguingly include various kinesin motors (Gruneberg et al., 2006; Kurasawa et al., 2004; Zhu and Jiang, 2005) and a RhoA GAP (Ban et al., 2004), may associate with PRC1 for ATP-independent transport to the spindle midzone. In addition, other spindle midzone components like the centralspindlin complex (Hizlan et al., 2006) may similarly use multiple antiparallel-oriented MT binding sites for their localization.

Apart from aiding localization, a polarity bias in MT crosslinking also enables ase1p to polarize self-organization processes. Newly nucleated MTs along interphase MT bundles, for example, are orientated antiparallel with respect to the underlying MT (Janson et al., 2005), even in the absence of klp2p (Figure S1B). This geometry, which may in part be initiated by a preferred orientation of nucleation complexes, is stabilized specifically by ase1p (see model, Figure 6A). In computer model 2, where ase1p has no polarity preference, MTs become oriented

randomly (Figure S5 and Movie S16) and, compared to model 1, the symmetry of the bundle-midzone is consequently decreased by almost a factor of 2 when the unbundled model is used as a baseline (Figure 5D). Previously, a parallel bias in crosslinking for the motors dynein and HSET was, based on computer simulations, proposed to aid the formation of monopolar asters out of randomly oriented MTs (Chakravarty et al., 2004). We can now imagine that in order to construct a complete bipolar spindle out of dispersedly nucleated MTs, cells use two different sets of bundlers and motors. One only interacts with parallel MTs and takes care of focusing MT minus ends into spindle poles, while the other interacts with antiparallel MTs and organizes the spindle midzone (see model, Figure 6B). Because of the difference in polarity bias, these two sorting systems may have very little crosstalk, e.g., the bundling of antiparallel MTs by ase1p during anaphase would not hinder the sorting of parallel MTs elsewhere. Ase1p can therefore act as a selective brake on motors that slide antiparallel MTs. In this light, it will be key to investigate the polarity preference of other mitotic motors and bundlers like Eg5 and NuMA.

MT End Tracking of Motors Creates Responsive MT Networks

How do cells regulate which MTs slide and which MTs are stably connected? Seemingly, when bundlers and motors accumulate between two MTs proportional to the amount of overlap, either sliding forces or bundling forces dominate, and MTs either slide or are immobile. Here, we

observed ase1p and klp2p disproportionally along MTs since ase1p localized along the full length of bundled MTs while klp2p accumulated only at MT plus ends (see model, Figure 6A). The molecular tug-of-war between ase1p and klp2p therefore resulted in a net sliding force that decreased with MT length. Computer simulations indicated that the bundling strength of ase1p can be made strong enough to create a bundle-midzone that resists compression forces by MT polymerization yet is weak enough to enable MT sliding of short MTs. Additionally, klp2p localization to MT plus ends made sliding a position-dependent process, since MT sliding stopped when a MT plus end moved beyond the bundle midzone. Sliding of MTs within long MT bundles occurs in various cell types, including neurons (Baas et al., 2006), mature megakaryocytes (Patel et al., 2005), and *Ustilago maydis* (Straube et al., 2006). Interestingly, observations in neurons show that, similarly to *S. pombe*, only short MTs are motile whereas longer MTs are stationary. We can thus imagine that end tracking of motors is a more commonly used strategy that allows for dynamic sorting of short MTs on one hand and the establishment of stable MT contacts on the other hand.

In particular, our work suggests how ase1p/PRC1 and molecular motors collaborate to regulate the overlap between antiparallel MT plus ends, such as those found in the spindle midzone. Like klp2p, kinesin-14 homologs in *Drosophila* (Goshima et al., 2005), *S. cerevisiae* (Sproul et al., 2005), and plant cells (Ambrose et al., 2005) have recently been shown to localize selectively to MT plus ends. The sliding forces that are produced by kinesin-14 family members or possible other plus-end-tracking motors between antiparallel MTs may therefore be overlap independent, whereas ase1p/PRC1 will generate length-dependent friction forces (see model, Figure 6B). In addition, plus-end-directed motors (such as MKLP1) may also accumulate between MTs in an overlap-dependent manner. As a result, there will be a net force that drives MT plus ends of opposing MTs toward each other when the overlap region is large, whereas for small overlap, minus-end-directed motors will dominate to slide plus ends away from each other. Our work therefore shows that several regulatory mechanisms become possible when motors are targeted to MT ends. It will be interesting to learn whether direct molecular interactions between ase1p/PRC1 and motors (Gruneberg et al., 2006; Kurasawa et al., 2004; Zhu and Jiang, 2005) play an additional role in the balancing of forces in MT overlap regions.

EXPERIMENTAL PROCEDURES

Genetic Methods
Standard media and genetic methods were used as described in the Nurse Lab Handbook (http://www.sanger.ac.uk/PostGenomics/ S_pombe/links.shtml#pombe). Plasmids and strains used are listed in Tables S1 and S2. Regions downstream and upstream of the intron in the *ase1* locus were separately amplified from *S. pombe* genomic DNA by PCR and simultaneously cloned into an expression vector. The upstream region was used to create truncated *ΔNase1* (amino

acids 143–731). *Ase1* and *ΔNase1* with an N terminus GFP tag where integrated into the *ura4* locus for FRAP and immunoprecipitation experiments (Figures 3D and S4B). GFP-tubulin and mRFP-tubulin were expressed from plasmids under the control of the inducible *nmt1* promoter. See Supplemental Experimental Procedures for details.

In Vitro Assays
Reagents were obtained from Sigma unless otherwise stated. GST-ase1 for Figure 3A was expressed in *E. coli*, immobilized on glutathione-Sepharose beads (Amersham), and eluted in 50 mM Tris and 10 mM reduced glutathione (pH 8) (see Supplemental Experimental Procedures and Figure S4A for details). Porcine tubulin and *Lytechinus pictus* axonemes were obtained as described previously (Tran et al., 1997). Coverslips were cleaned overnight in a saturated solution of KOH in ethanol and washed in water. A flowcell with an approximate volume of 5 μl was constructed by squeezing two lines of vacuum grease between a glass slide and a coverslip. Axonemes bound nonspecifically to the coverslip and the flowcell was flushed with 20 μl BSA in acetate buffer (pH 5.2; 50 mg/ml) to prevent excessive binding of GST-ase1p to the surface. After a flush with 20 μl MRB80 (80 mM K-PIPES, 1 mM EGTA, 4 mM MgCl$_2$ [pH 6.8]), 10 μl of polymerization/bundling mix was introduced (2 mg/ml tubulin, 1 mM GTP, and 0.5 mg/ml GST-ase1p in MRB80).

Ase1-GFP for Figure 3E was expressed in *E. coli* with an N-terminal 6× His tag, immobilized on Ni-NTA agarose (Qiagen) and eluted with 20 mM NaH$_2$PO$_4$, 500 mM NaCl, and 500 μM imidazole (pH 7.4). Proteins were spun 10 min in an airfuge (15 psi) directly before use to remove protein aggregates. Stabilized fluorescent MT seeds were grown by polymerizing 0.5 mg/ml tubulin (approximately a 1:1 mix between unlabeled and Cy5 monoreactive dye-labeled tubulin—Amersham) with 0.5 mM dtt and 0.2 mM GMPCPP (Jena Bioscience) at 34°C for 30 min in MRB80. Resulting MTs were diluted 60 times and extended with a short rhodamine-region at their plus ends by polymerization in 0.008 mg/ml TAMRA (Molecular Probes)-labeled tubulin, 0.04 unlabeled tubulin, 0.03 NEM-treated tubulin, 0.5 mM dtt, 0.1 mM GMPCPP, and 10 μM taxol for 10 min at 23°C. Cleaned coverslips were made hydrophobic with a dimethyldichlorosilane treatment (15 min in 1 v/v % dds in trichloroethylene [Kapitein et al., 2005]), and a flowcell was created. Unlabeled GST-ase1p (0.5 mg/ml in MRB80) was immobilized on the coverslip, and the flowcell was flushed with 20 μl BSA (50 mg/ml in MRB80) to remove excess GST-ase1p and to further block vacant sites. MT seeds were mixed with 16 μg/ml His-ase1-GFP in MRB80 and introduced into the flowcell. The MT binding sites of immobilized GST-ase1p bound the MTs to the surface, which aided observation.

The N terminus of sequence ase1p (first 483 amino acids) was cloned into the ligation-independent cloning vector pETHSUL (S.D. Weeks, personal communication) for expression in *E. coli*. The N-terminal 6× His tag, used for purification, was cleaved with SUMO protease. Proteins were dialyzed against MRB80 and crosslinked with varying amounts of EGS; Ethylene glycol bis(succinimidyl succinate).

Image Acquisition and Analysis
Details on preparation of *S. pombe* cells and image acquisition can be found in the Supplemental Experimental Procedures. All imaging was done at room temperature (close to 23°C), except for FRAP measurements, which were done at 27°C.

Metamorph was used for generating kymographs of image areas (typically 200 by 20 pixels) that contained a single MT bundle. The maximum pixel intensity of each 20 pixels is displayed along a horizontal line (200 pixels long) for each time point.

The average intensity of frapped regions (I$_{FRAP}$), which position on the MT bundle was tracked in time using kymographs, was corrected for background intensity and overall bleaching due to subsequent imaging. Bleaching was estimated from a nonfrapped region (I$_{CONTROL}$).

Background intensity levels (I_{BGR}) were measured outside the cell. The corrected signal $(I_{FRAP}(t) - I_{BGR}) \times (I_{CONTROL\_before\_FRAP} - I_{BGR})/(I_{CONTROL}(t) - I_{BGR})$ was fitted with a single exponential $A - B \exp(-t/\tau)$ to obtain the recovery time constant.

Velocities and lengths of sliding MTs (Figure 5C) were obtained from kymographs. On the kymographs, lines were drawn along the MT plus and minus ends and along a speckle on the underlying MT. The distance between these lines at each time point indicated relative sliding and MT length. In vitro, growing MT plus ends could be distinguished from minus ends based on their higher growth velocity (1.60 ± 0.05 µm/min and 0.26 ± 0.02 µm/min; $\pm$SEM; n = 16 for both). Time-lapsed images (0.5 fps) of growing MTs were systematically scanned for growing MTs that crossed or bundled existing MTs. All encounters, for which the interaction angle was smaller than 45 degrees and for which MT polarity could be established, were analyzed. The vast majority of interactions with angles larger than 45 degrees did not bundle. Bundle probability of polarity-marked seeds was addressed by counting only combinations of two MTs that showed a bundled region flanked by two single MT regions.

Computer Simulations

Computer simulations solved the overdamped Langevin equation for MTs (See Table S3 for parameter values and Supplemental Experimental Procedures for details). MTs diffused in a confined space where, except for the unbundled model, motor proteins (klp2p), bundling proteins (ase1p), and nucleation complexes (NCs) were present. MT plus ends exhibited dynamic instability without MT rescues. We mimicked the mechanical constraints imposed on MTs by the cell wall using variable growth and catastrophe rates.

Protein complexes were modeled by two MT binding domains connected by a Hookean link. Binding domains bound MTs within a distance of 20 nm with a specified attachment rate. Detachment occurred stochastically at a given rate but was additionally force sensitive according to $p_{detach} = p_0 \exp(f/f_s)$, where f_s is the typical strength of binding. Klp2p consisted of a domain that attached within a short distance of the MT plus end and a domain that could travel along another antiparallel MT at a force-dependent speed. Ase1p was modeled by two identical binding domains with the optional restriction of binding MTs of opposite orientation. Nucleation complexes (NCs) consisted of an activating domain and a nucleating domain. When the activating domain was bound to an existing MT, the nucleating domain could create a new MT with a given nucleation rate. The nucleating domain remained occupied by the minus end of the new MT until this MT completely depolymerized, at which point the NC was again capable of nucleation. Simulations were started by nucleating once a single MT from an unbound NC. In the unbundled model, nucleation occurred stochastically at random locations, independent of other MTs present.

Supplemental Data

Supplemental Data include six figures, three tables, eight movies, Supplemental Experimental Procedures, and compiled simulation code (Mac and PC versions)—an explanatory README file is provided—and can be found with this article online at http://www.cell.com/cgi/content/full/128/2/357/DC1/.

REFERENCES

Ambrose, J.C., Li, W.X., Marcus, A., Ma, H., and Cyr, R. (2005). A minus-end-directed kinesin with plus-end trackin protein activity is involved in spindle morphogenesis. Mol. Biol. Cell *16*, 1584–1592.

Baas, P.W., Vidya Nadar, C., and Myers, K.A. (2006). Axonal transport of microtubules: the long and short of it. Traffic *7*, 490–498.

Ban, R., Irino, Y., Fukami, K., and Tanaka, H. (2004). Human mitotic spindle-associated protein PRC1 inhibits MgcRacGAP activity toward Cdc42 during the metaphase. J. Biol. Chem. *279*, 16394–16402.

Brunner, D., and Nurse, P. (2000). CLIP170-like tip1p spatially organizes microtubular dynamics in fission yeast. Cell *102*, 695–704.

Carazo-Salas, R.E., and Nurse, P. (2006). Self-organization of interphase microtubule arrays in fission yeast. Nat. Cell Biol. *8*, 1102–1107.

Carazo-Salas, R.E., Antony, C., and Nurse, P. (2005). The kinesin Klp2 mediates polarization of interphase microtubules in fission yeast. Science *309*, 297–300.

Chakravarty, A., Howard, L., and Compton, D.A. (2004). A mechanistic model for the organization of microtubule asters by motor and non-motor proteins in a mammalian mitotic extract. Mol. Biol. Cell *15*, 2116–2132.

Daga, R.R., Lee, K.-G., Bratman, S., Salas-Pino, S., and Chang, F. (2006). Self-organization of microtubule bundles in anucleate fission yeast cells. Nat. Cell Biol. *8*, 1108–1113.

Djinovic-Carugo, K., Young, P., Gautel, M., and Saraste, M. (1999). Structure of the alpha-actinin rod: Molecular basis for crosslinking of actin filaments. Cell *98*, 537–546.

Drummond, D.R., and Cross, R.A. (2000). Dynamics of interphase microtubules in *Schizosaccharomyces pombe*. Curr. Biol. *10*, 766–775.

Goshima, G., Nedelec, F., and Vale, R.D. (2005). Mechanisms for focusing mitotic spindle poles by minus end-directed motor proteins. J. Cell Biol. *171*, 229–240.

Gruneberg, U., Neef, R., Li, X.L., Chan, E.H.Y., Chalamalasetty, R.B., Nigg, E.A., and Barr, F.A. (2006). KIF14 and citron kinase act together to promote efficient cytokinesis. J. Cell Biol. *172*, 363–372.

Heald, R., Tournebize, R., Blank, T., Sandaltzopoulos, R., Becker, P., Hyman, A., and Karsenti, E. (1996). Self-organization of microtubules into bipolar spindles around artificial chromosomes in Xenopus egg extracts. Nature *382*, 420–425.

Heidemann, S., Landers, J., and Hamborg, M. (1981). Polarity orientation of axonal microtubules. J. Cell Biol. *91*, 661–665.

Hizlan, D., Mishima, M., Tittmann, P., Gross, H., Glotzer, M., and Hoenger, A. (2006). Structural analysis of the ZEN-4/CeMKLP1 motor domain and its interaction with microtubules. J. Struct. Biol. *153*, 73–84.

Janson, M.E., Setty, T.G., Paoletti, A., and Tran, P.T. (2005). Efficient formation of bipolar microtubule bundles requires microtubule-bound γ-tubulin complexes. J. Cell Biol. *169*, 297–308.

Kapitein, L.C., Peterman, E.J.G., Kwok, B.H., Kim, J.H., Kapoor, T.M., and Schmidt, C.F. (2005). The bipolar mitotic kinesin Eg5 moves on both microtubules that it crosslinks. Nature *435*, 114–118.

Kurasawa, Y., Earnshaw, W.C., Mochizuki, Y., Dohmae, N., and Todokoro, K. (2004). Essential roles of KIF4 and its binding partner PRC1 in organized central spindle midzone formation. EMBO J. *23*, 3237–3248.

Loiodice, I., Staub, J., Setty, T.G., Nguyen, N.P.T., Paoletti, A., and Tran, P.T. (2005). Ase1p organizes antiparallel microtubule arrays during interphase and mitosis in fission yeast. Mol. Biol. Cell *16*, 1756–1768.

Mahoney, N.M., Goshima, G., Douglass, A.D., and Vale, R.D. (2006). Making microtubules and mitotic spindles in cells without functional centrosomes. Curr. Biol. *16*, 564–569.

Maresca, T.J., Niederstrasser, H., Weis, K., and Heald, R. (2005). Xnf7 contributes to spindle integrity through its microtubule-bundling activity. Curr. Biol. *15*, 1755–1761.

Merdes, A., Ramyar, K., Vechio, J.D., and Cleveland, D.W. (1996). A complex of NuMA and cytoplasmic dynein is essential for mitotic spindle assembly. Cell *87*, 447–458.

Meyer, R.K., and Aebi, U. (1990). Bundling of actin-filaments by alpha-actinin depends on its molecular length. J. Cell Biol. *110*, 2013–2024.

Mollinari, C., Kleman, J.P., Jiang, W., Schoehn, G., Hunter, T., and Margolis, R.L. (2002). PRC1 is a microtubule binding and bundling protein essential to maintain the mitotic spindle midzone. J. Cell Biol. *157*, 1175–1186.

Murata, T., Sonobe, S., Baskin, T.I., Hyodo, S., Hasezawa, S., Nagata, T., Horio, T., and Hasebe, M. (2005). Microtubule-dependent microtubule nucleation based on recruitment of gamma-tubulin in higher plants. Nat. Cell Biol. *7*, 961–968.

Nedelec, F. (2002). Computer simulations reveal motor properties generating stable antiparallel microtubule interactions. J. Cell Biol. *158*, 1005–1015.

Nislow, C., Lombillo, V.A., Kuriyama, R., and McIntosh, J.R. (1992). A plus-end-directed motor enzyme that moves antiparallel microtubules in vitro localizes to the interzone of mitotic spindles. Nature *359*, 543–547.

Patel, S.R., Richardson, J.L., Schulze, H., Kahle, E., Galiart, N., Drabek, K., Shivdasani, R.A., Hartwig, J.H., and Italiano, J.E. (2005). Differential roles of microtubule assembly and sliding in proplatelet formation by megakaryocytes. Blood *106*, 4076–4085.

Sagolla, M.J., Uzawa, S., and Cande, W.Z. (2003). Individual microtubule dynamics contribute to the function of mitotic and cytoplasmic arrays in fission yeast. J. Cell Sci. *116*, 4891–4903.

Schuyler, S.C., Liu, J.Y., and Pellman, D. (2003). The molecular function of Ase1p: evidence for a MAP-dependent midzone-specific spindle matrix. J. Cell Biol. *160*, 517–528.

Sharp, D., Kuriyama, R., Essner, R., and Baas, P. (1997). Expression of a minus-end-directed motor protein induces Sf9 cells to form axon-like processes with uniform microtubule polarity orientation. J. Cell Sci. *110*, 2373–2380.

Sharp, D.J., Rogers, G.C., and Scholey, J.M. (2000). Microtubule motors in mitosis. Nature *407*, 41–47.

Smertenko, A.P., Chang, H.Y., Wagner, V., Kaloriti, D., Fenyk, S., Sonobe, S., Lloyd, C., Hauser, M.T., and Hussey, P.J. (2004). The Arabidopsis microtubule-associated protein AtMAP65-1: Molecular analysis of its microtubule bundling activity. Plant Cell *16*, 2035–2047.

Sproul, L.R., Anderson, D.J., Mackey, A.T., Saunders, W.S., and Gilbert, S.P. (2005). Cik1 targets the minus-end kinesin depolymerase Kar3 to microtubule plus ends. Curr. Biol. *15*, 1420–1427.

Straube, A., Hause, G., Fink, G., and Steinberg, G. (2006). Conventional kinesin mediates microtubule-microtubule interactions in vivo. Mol. Biol. Cell *17*, 907–916.

Tran, P.T., Walker, R.A., and Salmon, E.D. (1997). A metastable intermediate state of microtubule dynamic instability that differs significantly between plus and minus ends. J. Cell Biol. *138*, 105–117.

Tran, P.T., Marsh, L., Doye, V., Inoue, S., and Chang, F. (2001). A mechanism for nuclear positioning in fission yeast based on microtubule pushing. J. Cell Biol. *153*, 397–411.

Waterman-Storer, C.M., Desai, A., Bulinski, J.C., and Salmon, E.D. (1998). Fluorescent speckle microscopy, a method to visualize the dynamics of protein assemblies in living cells. Curr. Biol. *8*, 1227–1230.

Yamashita, A., Sato, M., Fujita, A., Yamamoto, M., and Toda, T. (2005). The roles of fission yeast Ase1 in mitotic cell division, meiotic nuclear oscillation, and cytokinesis checkpoint signaling. Mol. Biol. Cell *16*, 1378–1395.

Zhu, C., Lau, E., Schwarzenbacher, R., Bossy-Wetzel, E., and Jiang, W. (2006). Spatiotemporal control of spindle midzone formation by PRC1 in human cells. Proc. Natl. Acad. Sci. USA *103*, 6196–6201.

Zhu, C.J., and Jiang, W. (2005). Cell cycle-dependent translocation of PRC1 on the spindle by Kif4 is essential for midzone formation and cytokinesis. Proc. Natl. Acad. Sci. USA *102*, 343–348.